

# Multi-species modeling in the particle-based ESBGK method for monatomic gas species

M. Pfeiffer,<sup>1, a)</sup> A. Mirza,<sup>2, b)</sup> and P. Nizenkov<sup>2, c)</sup>

<sup>1)</sup>*Institute of Space Systems, University of Stuttgart, Pfaffenwaldring 29, D-70569 Stuttgart, Germany*

<sup>2)</sup>*boltzplatz - Numerical Plasma Dynamics, Technology Transfer Initiative GmbH at the University of Stuttgart, Nobelstraße 15, 70569 Stuttgart, Germany*

(Dated: 19 November 2020)

Multi-species modeling is implemented for the particle-based ellipsoidal statistical Bhatnagar-Gross-Krook (ESBGK) for monatomic species in the open-source plasma simulation suite PICLas. After a literature review on available multi-species extensions of the kinetic model equations and approaches for the determination of the transport coefficients, Brull's model is implemented for the former and Wilke's mixing rules and collision integrals for the latter. The implementation is verified with three simulation test cases: a simple reservoir, a supersonic Couette flow and the hypersonic flow around a 70° blunted cone. The simulation results are compared with the Direct Simulation Monte Carlo (DSMC) method, where good overall agreement can be achieved. However, the determination of the transport coefficients through collision integrals offers better agreement with the DSMC results at acceptable computational cost. For the last test case, a comparison of the computational duration is presented.

Keywords: DSMC, Ellipsoidal statistical BGK, Multi-species, Mixture

## I. INTRODUCTION

Numerical simulations of fluid dynamics in space applications such as atmospheric entry maneuvers and in-space propulsion systems pose considerable challenges for the applied numerical methods. Large density gradients spanning from the continuum regime to the free molecular flow and the consequent breakdown of the continuum assumption require the utilization of numerical methods with an extended applicability. A well-established method for the simulation of rarefied gas flows is the Direct Simulation Monte Carlo (DSMC) method<sup>1</sup>. Although applicable in the continuum regime, the microscopic treatment of the gas flow becomes computationally infeasible. Thus, a coupling of DSMC with a computationally efficient method is desirable. While conventional computational fluid dynamics (CFD) approaches based on the solution of the Navier-Stokes equations offer a fast numerical solution in the continuum regime, the bidirectional coupling with the DSMC method is cumbersome due to the utterly different approaches of the methods<sup>2</sup>. Recently, particle-based continuum methods gained traction as an alternative solution, bridging the gap in the transitional regime. A recent review of several such methods was conducted by Pfeiffer, Mirza, and Nizenkov<sup>3</sup>.

One of the most promising approaches is the Bhatnagar-Gross-Krook model<sup>4</sup>, which is an approximation of the collision integral of the Boltzmann equation. The assumption is that the distribution function relaxes

towards a target distribution function, which can have different forms. While the original BGK model using the Maxwellian distribution cannot reproduce the correct Prandtl numbers, different alternative distribution functions exist. Two popular functions are used for the simulation of rarefied gas flows in high-speed applications: the Ellipsoidal Statistical (ESBGK)<sup>5</sup> and Shakhov (SBGK)<sup>6</sup> models. In the continuum limit, both methods can be used to derive the Navier-Stokes equations. While both models have been implemented in PICLas<sup>7,8,9</sup> and extensively tested for atmospheric re-entry<sup>10</sup> and nozzle expansion<sup>3</sup> flows in the particle-based context, this has been done for single component gases. The focus in this paper is the extension of the particle-based ESBGK model to gas mixtures. For this purpose, two major challenges have to be addressed.

### A. Extension of the kinetic model equations

First, a proper mathematical model is required which fulfills the consistency requirements of the Boltzmann collision operator such as conservation, equilibrium, H-theorem and positivity of the density and temperature fields. Moreover, it has to satisfy the indifferenciability principle<sup>11</sup>, meaning that in case of identical species in terms of masses and cross-sections, the total distribution function reduces to the single species system. Finally, these models have to be able to correctly reproduce the transport coefficients (diffusion by Fick's law, viscous stress by Newton's law, and thermal conductivity by Fourier's law) in the continuum limit. Available models can be categorized based on the treatment of the collision term<sup>12</sup>: single- and multi-relaxation modeling, where the difference is whether a single or multiple relax-

<sup>a)</sup>Electronic mail: mpfeiffer@irs.uni-stuttgart.de

<sup>b)</sup>Electronic mail: mirza@boltzplatz.eu

<sup>c)</sup>Electronic mail: nizenkov@boltzplatz.eu

ation rates are employed for self- and cross-collisions. On the one hand, single-relaxation models are computationally more efficient and less complex than multi-relaxation models. On the other hand, multi-relaxation models with different relaxation rates are likely to be better suited for mixtures, where the species differ substantially. Since many of the models were derived mathematically but not applied to a realistic application, it is not clear whether the more complex multi-relaxation model are absolutely required for most of the application cases. Therefore, the focus of this project will be on single-relaxation models. However, Klingenberg, Pirner, and Puppo<sup>13</sup> are developing a potential multi-relaxation model, which might be considered in future work.

Single-relaxation models for the ESBGK model, which satisfy the indifferentiability principle, were introduced by Groppi, Monica, and Spiga<sup>14</sup> and Brull<sup>15</sup>, extending the ideas introduced by Andries, Aoki, and Perthame<sup>11</sup> for the original BGK model. The model by Groppi, Monica, and Spiga<sup>14</sup> is able to reproduce the correct diffusion coefficient and viscous stress and the model by Brull<sup>15</sup> is able to reproduce the correct viscous stress and thermal conductivity. To rectify the shortcomings, Todorova and Steijl<sup>16</sup> introduced an extension to the model by Groppi, Monica, and Spiga<sup>14</sup> to reproduce the correct thermal conductivity in the continuum limit by adding an additional free parameter. The focus of this paper is Brull's model with two different approaches for the determination of the transport coefficients.

## B. Determination of the transport coefficients for mixtures

Second, a method for the determination of transport coefficients of the gas mixture has to be devised. Here, much of the work done for conventional computational fluid dynamics can be capitalized on. One of the most widely used approaches are the mixing rules by Wilke<sup>17</sup>, which were derived from kinetic gas theory. Palmer and Wright<sup>18</sup> gives an overview of available mixing rules and approximative methods to determine transport coefficients, including a comparison of Wilke's mixing rules with two more advanced models. A more recent approach with fewer assumptions is to calculate the transport coefficients directly from collision integrals as outlined by Hirschfelder, Curtiss, and Bird<sup>19</sup>. For this purpose, different fits for the collision integrals can be utilized to speed up calculation times (e.g. by Kestin *et al.*<sup>20</sup>, Capitelli *et al.*<sup>21</sup>, and Wright *et al.*<sup>22</sup>, Wright, Hwang, and Schwenke<sup>23</sup>, who give an overview over the available collision integral data for the atmospheres of Earth, Mars, and Venus). Most of these collision integrals assume an attractive-repulsive intermolecular potential. However, to allow for a comparison with the Direct Simulation Monte Carlo method in PICLas, either collision integrals using the Variable Hard Sphere (VHS) have to be implemented as given by Stephani,

Goldstein, and Varghese<sup>24</sup> or a collision model using the Lennard-Jones potential has to be implemented in the DSMC method as presented by Venkatraman and Alexeenko<sup>25</sup>. The former approach is chosen for this paper.

## II. THEORY

The Boltzmann equation describes the gas kinetic behavior of the particle distribution function  $f_s = f(\mathbf{x}, \mathbf{v}, t)$  at position  $\mathbf{x}$  and velocity  $\mathbf{v}$  of the species  $s$

$$\frac{\partial f_s}{\partial t} + \mathbf{v} \cdot \frac{\partial f_s}{\partial \mathbf{x}} = \frac{\delta f_s}{\delta t} \Big|_{\text{coll}}, \quad (1)$$

where external forces are neglected. Furthermore,  $\delta f_s / \delta t|_{\text{coll}}$  is the collision term for a mixture of  $M$  gases, which can be described by the Boltzmann collision integral

$$\frac{\partial f_s}{\partial t} \Big|_{\text{coll}} = \sum_{k=1}^M \int_{\mathbb{R}^3} \int_{S^2} \mathcal{B}_{s,k} [f_s(\mathbf{v}') f_k(\mathbf{v}'_*) - f_s(\mathbf{v}) f_k(\mathbf{v}_*)] d\mathbf{n} d\mathbf{v}_*. \quad (2)$$

Here,  $S^2 \subset \mathbb{R}^3$  is the unit sphere,  $\mathbf{n}$  is the unit vector of the scattered velocities,  $\mathcal{B}_{s,k}$  is the collision kernel and the superscript  $'$  denotes the post-collision velocities. The multiple integration of this collision term makes it difficult to compute. The macroscopic flow values particle density  $n$ , flow velocity  $u$  and temperature  $T$  of each species  $s$  are defined as:

$$n_s = \int_{\mathbb{R}^3} f_s d\mathbf{v}, \quad n_s \mathbf{u}_s = \int_{\mathbb{R}^3} \mathbf{v} f_s d\mathbf{v}, \quad (3)$$

$$\mathcal{E}_s = \frac{3}{2} k_B T_s = \frac{m_s}{2n_s} \int_{\mathbb{R}^3} \mathbf{c}_s^2 f_s d\mathbf{v}, \quad (4)$$

$$E_s = \frac{1}{2} m_s n_s \mathbf{u}_s^2 + n_s \mathcal{E}_s, \quad (5)$$

with the thermal particle velocity  $\mathbf{c}_s = \mathbf{v} - \mathbf{u}_s$ . Furthermore, the macroscopic mean values of the flow are given by:

$$n = \sum_{k=1}^M n_k, \quad \rho = \sum_{k=1}^M m_k n_k, \quad \rho \mathbf{u} = \sum_{k=1}^M m_k n_k \mathbf{u}_k, \quad (6)$$

$$n \mathcal{E} + \frac{\rho}{2} \mathbf{u}^2 = E = \sum_{k=1}^M E_k, \quad \mathcal{E} = \frac{3}{2} k_B T. \quad (7)$$

### A. ESBGK Mixture Model

The ESBGK mixture model of Brull<sup>15</sup> approximates the collision term using one relaxation term per species, where the distribution function relaxes towards a target

distribution function  $f_s^{\text{ES}}$  with a certain relaxation frequency  $\nu$ :

$$\left. \frac{\partial f_s}{\partial t} \right|_{\text{coll}} = \nu (f_s^{\text{ES}} - f_s). \quad (8)$$

The target velocity distribution function  $f_s^{\text{ES}}$  is given by

$$f_s^{\text{ES}} = \frac{n_s}{\sqrt{\det \mathcal{A}}} \left( \frac{m_s}{2\pi k_B T} \right)^{3/2} \exp \left[ -\frac{m_s \mathbf{c}^T \mathcal{A}^{-1} \mathbf{c}}{2k_B T} \right] \quad (9)$$

with the anisotropic matrix

$$\mathcal{A} = \mathcal{I} - \frac{1 - \alpha Pr}{\alpha Pr} \left( \frac{\mathcal{P}}{k_B T / m} - \mathcal{I} \right). \quad (10)$$

The anisotropic matrix  $\mathcal{A}$  consists of the identity matrix  $\mathcal{I}$  and the pressure tensor  $\mathcal{P}$ ,

$$\mathcal{P} = \frac{1}{\rho} \sum_{k=1}^M m_k \int (\mathbf{v} - \mathbf{u})(\mathbf{v} - \mathbf{u})^T f_k d\mathbf{v}, \quad (11)$$

which are both symmetric. Additionally,  $\mathbf{c} = \mathbf{v} - \mathbf{u}$  is the thermal particle velocity determined from the particle velocity  $\mathbf{v}$  and the average flow velocity  $\mathbf{u}$ .  $Pr$  is the targeted Prandtl number of the gas mixture and  $\alpha$  is a mass fraction and density fraction dependent variable of the model

$$\alpha = \sum_{k=1}^M \frac{n_k}{n} \frac{m}{m_k}, \quad m = \sum_{k=1}^M \frac{n_k}{n} m_k. \quad (12)$$

The relaxation frequency  $\nu$  of the model is defined by

$$\nu = \frac{n k_B T}{\mu} \alpha Pr \quad (13)$$

with the viscosity of the mixture  $\mu$ . The ESBGK model of Brull<sup>15</sup> produces a positive definite matrix  $\mathcal{A}$  for Prandtl numbers in the range of  $[\frac{2}{3\alpha}, \infty[$ , which depends on the involved species masses and the mole fractions. More precisely, this condition is too restrictive according to Mathiaud and Mieussens<sup>26</sup>. It is demonstrated that the matrix is positive definite as long as the Prandtl number used in the scheme  $Pr^*$  is chosen as

$$\alpha Pr^* = \frac{1}{1 - \tilde{\nu}}, \quad (14)$$

$$\tilde{\nu} = \max \left( 1 - \frac{1}{\alpha Pr}, -\frac{k_B T / m}{\lambda_{max} - k_B T / m} \right), \quad (15)$$

with  $\lambda_{max}$  being the maximum eigenvalue of  $\mathcal{P}$ . Nevertheless, in every simulation of this paper the case never occurred that the target Prandtl number could not be reached. The Brull-ESBGK model for mixtures reproduces the Maxwellian distribution in the equilibrium state and fulfills the H-theorem. Furthermore, it fulfills the indifferentiability principle which means that the model reduces to a single species model for identical species<sup>15</sup>.

## B. Gas mixture properties

For the calculation of the gas mixture viscosity assuming a variable hard sphere (VHS) interaction potential, two different approaches are tested: the approximation of the mixture properties using Wilke's mixture rules<sup>17</sup> and the first approximation of the transport properties using collision integrals<sup>19</sup>.

### 1. Wilke's mixing rules

For this approach, the well known exponential ansatz of the viscosity  $\mu_k$

$$\mu_k = \mu_{\text{ref},k} \left( \frac{T_k}{T_{\text{ref},k}} \right)^{\omega_{\text{VHS},k}} \quad (16)$$

is used for each species  $k$ . Here,  $T_{\text{ref}}$ , is a reference temperature,  $\mu_{\text{ref},k}$  the reference dynamic viscosity at  $T_{\text{ref},k}$ <sup>27</sup> and  $\omega_{\text{VHS},k}$  is a parameter of the VHS model. For a VHS gas the reference dynamic viscosity can be calculated with the VHS reference diameter  $d_{\text{ref},k}$ :

$$\mu_{\text{ref},k} = \frac{30 \sqrt{m_k k_B T_{\text{ref},k}}}{4 \sqrt{\pi} (5 - 2\omega_{\text{VHS},k}) (7 - 2\omega_{\text{VHS},k}) d_{\text{ref},k}^2}. \quad (17)$$

The mixture viscosity is calculated using Wilke's mixture rule<sup>17</sup>:

$$\mu = \sum_{k=1}^M n_k \frac{\mu_k}{\Phi_k}, \quad \Phi_k = \sum_{r=1}^M n_r \frac{\left( 1 + \sqrt{\frac{\mu_k}{\mu_r}} \left( \frac{m_r}{m_k} \right)^{1/4} \right)^2}{\sqrt{8 \left( 1 + \frac{m_k}{m_r} \right)}}. \quad (18)$$

The Prandtl number of the gas mixture is defined as

$$Pr = c_p \frac{\mu}{K} \quad (19)$$

with the thermal conductivity  $K$  of the mixture and the specific heat  $c_p = \frac{5k_B}{2m}$  evaluated with the mixture mass  $m$ . The thermal conductivity of each species  $K_k$  is calculated using the Eucken's relation with the viscosity<sup>18</sup>:

$$K_k = \frac{15}{4} \frac{\mu_k k_B}{m_k}. \quad (20)$$

Afterwards, the thermal conductivity of the mixture  $K$  is again calculated using Wilke's mixture rule:

$$K = \sum_{k=1}^M n_k \frac{K_k}{\Phi_k}. \quad (21)$$

### 2. First approximation of transport properties

The first approximation to the viscosity of species  $k$  depending on the collision integral  $\Omega_k^{(2)}$  (2) is given by<sup>19</sup>

$$\mu_k = \frac{5k_B T}{8\Omega_k^{(2)}(2)}. \quad (22)$$

The mixture viscosity is determined by

$$\mu = \sum_{k=1}^M b_k, \quad (23)$$

where  $b_k$  is the contribution of each species to the total mixture viscosity and is determined by solving the system

$$\chi_k = b_k \left( \frac{\chi_k}{\mu_k} + \sum_{r \neq k} \frac{3\chi_r}{(\rho'_r + \rho'_k) D_{kr}} \left( \frac{2}{3} + \frac{m_r}{m_k} A_{kr} \right) \right) - \chi_k \sum_{r \neq k} \frac{3b_r}{(\rho'_r + \rho'_k) D_{kr}} \left( \frac{2}{3} - A_{kr} \right) \quad (24)$$

with the mole fraction  $\chi$ , the density  $\rho'_r$  of species  $r$  when pure at pressure and temperature of the actual gas mixture, the parameter  $A_{kr}$  defined by

$$A_{kr} = \frac{\Omega_{kr}^{(2)}(2)}{5\Omega_{kr}^{(1)}(1)} \quad (25)$$

and the binary diffusion coefficient with the reduced mass  $m_{kr}^*$ :

$$D_{kr} = \frac{3k_B T}{16nm_{kr}^* \Omega_{kr}^{(1)}(1)}. \quad (26)$$

The mixture thermal conductivity  $K$  is calculated by

$$K = \sum_{k=1}^M a_k, \quad (27)$$

with  $a_k$  being the species contribution to the total mixture thermal conductivity. The factors  $a_k$  are determined by solving the system

$$\begin{aligned} \chi_k &= a_k \left[ \frac{\chi_k}{K_k} + \sum_{r \neq k} \frac{\chi_r}{5k_B n D_{kr}} \right. \\ &\times \left( 6 \left( \frac{m_k}{m_r + m_k} \right)^2 - (5 - 4B_{kr}) \left( \frac{m_r}{m_r + m_k} \right)^2 \right. \\ &\quad \left. \left. + 8 \frac{m_r m_k}{(m_k + m_r)^2} A_{kr} \right) \right] \\ &- \chi_k \sum_{r \neq k} a_r \frac{m_r m_k}{(m_k + m_r)^2} (5k_B n D_{kr})^{-1} \\ &\times (11 - 4B_{kr} - 8A_{kr}). \end{aligned} \quad (28)$$

Here,  $K_k$  is the first approximation of the thermal conductivity of species  $k$

$$K_k = \frac{25c_V k_B T}{16\Omega_k^{(2)}(2)}, \quad c_V = \frac{3k_b}{2m_k} \quad (29)$$

and the parameter  $B_{kr}$  is defined by

$$B_{kr} = \frac{5\Omega_{kr}^{(1)}(2) - \Omega_{kr}^{(1)}(3)}{5\Omega_{kr}^{(1)}(1)} \quad (30)$$

The collision integrals for the VHS model are given by Stephani, Goldstein, and Varghese<sup>24</sup>:

$$\begin{aligned} \Omega_{kr}^{\text{VHS},(1)}(1) &= \frac{\pi}{2} d_{\text{ref}}^2 \sqrt{\frac{k_B T}{2\pi m_{kr}^*}} \left( \frac{T_{\text{ref}}}{T} \right)^{\omega-1/2} \frac{\Gamma(7/2-\omega)}{\Gamma(5/2-\omega)} \\ \Omega_{kr}^{\text{VHS},(2)}(2) &= \frac{\pi}{3} d_{\text{ref}}^2 \sqrt{\frac{k_B T}{2\pi m_{kr}^*}} \left( \frac{T_{\text{ref}}}{T} \right)^{\omega-1/2} \frac{\Gamma(9/2-\omega)}{\Gamma(5/2-\omega)} \\ B_{kr}^{\text{VHS}} &= \frac{5\Gamma(9/2-\omega) - \Gamma(11/2-\omega)}{5\Gamma(7/2-\omega)}, \end{aligned} \quad (31)$$

with the VHS parameters  $d_{\text{ref}}$ ,  $T_{\text{ref}}$  and  $\omega$ .

### III. IMPLEMENTATION

The proposed ESBGK particle method for mixtures is implemented in the PIC-DSMC-BGK code PICLas<sup>28,29</sup> as described in detail by Pfeiffer<sup>8,9</sup>. The main concept of the particle ESBGK method, especially the energy and momentum conservation is based on the works of Gallis and Torczynski<sup>30,31</sup>. The ESBGK particle method has many similarities to the DSMC method: particles are moved on a simulation mesh, collide with boundaries and the microscopic particle properties are sampled to calculate macroscopic values in the same manner. But instead of performing binary collisions between particles, each particle of species  $s$  in a cell relaxes with the probability

$$P = 1 - \exp[-\nu \Delta t] \quad (32)$$

according to Eq. (8) towards the target distribution  $f_s^{\text{ES}}$ . For this, the relaxation frequency  $\nu$  is evaluated in each time step for each cell, depending on the targeted Prandtl number and the mixture viscosity in the cell.

A particle chosen to relax receives a new particle velocity sampled from the target distribution with the corresponding particle mass of the species. The detailed description of the sampling process for different target distributions (e.g. ESBGK or SBGK) can be found in Pfeiffer<sup>8</sup>. As proposed by Gallis and Torczynski<sup>30</sup>, a symmetric transformation matrix  $\mathcal{S}$  can be defined to describe the anisotropic matrix  $\mathcal{A}$  from Eq. (10):  $\mathcal{A} = \mathcal{S}\mathcal{S}$ . Furthermore, a normalized thermal velocity vector  $\mathbf{C}$  is defined as such that  $\mathbf{c} = \mathcal{S}\mathbf{C}$ . Using these definitions, the argument of the exponential function in Eq. (9) becomes

$$\mathbf{c}^T \mathcal{A}^{-1} \mathbf{c} = (\mathcal{S}\mathbf{C})^T \mathcal{S}^{-1} \mathcal{S}^{-1} \mathcal{S}\mathbf{C} = \mathbf{C}^T \mathbf{C} \quad (33)$$

using  $(\mathcal{S}\mathbf{C})^T = \mathbf{C}^T \mathcal{S}^T = \mathbf{C}^T \mathcal{S}$  due to the fact that  $\mathcal{S}$  is symmetric. Consequently,  $\mathcal{S}$  can transform a vector  $\mathbf{C}$  sampled from a Maxwellian distribution to a vector  $\mathbf{c}$  sampled from Eq. (9). Here, an approach is used with an approximation of the transformation matrix  $\mathcal{S}$  as described in previous studies<sup>8,27,30</sup>

$$\mathcal{S}_{ij} = \delta_{ij} - \frac{1 - \alpha Pr}{2\alpha Pr} \left[ \frac{m}{k_B T} \mathcal{P}_{ij} - \delta_{ij} \right]. \quad (34)$$

In the context of particle methods, the required moments are evaluated with

$$\mathcal{E}_s = \frac{1}{N_s - 1} \sum_{p=1}^{N_s} \frac{m_s}{2} (\mathbf{v}_{p,s} - \mathbf{u}_s)^2, \quad (35)$$

$$\begin{aligned} \mathcal{P} &= \frac{1}{(\sum_{s=1}^M \sum_{p=1}^{N_s} m_s)(N_{\text{total}} - 1)} \\ &\times \sum_{s=1}^M \sum_{p=1}^{N_s} m_s (\mathbf{v}_{p,s} - \mathbf{u})(\mathbf{v}_{p,s} - \mathbf{u})^T, \end{aligned} \quad (36)$$

with the particle number  $N_s$  per species  $s$  and the total particle number  $N_{\text{total}} = \sum_{s=1}^M N_s$ . Here, the factors  $\frac{1}{N_s-1}$  and  $\frac{1}{N_{\text{total}}-1}$  lead to an unbiasedness of the variance. It is obvious that at least two particles per species are needed to calculate the species temperature. However, this leads to a bad estimation of the temperature and it is recommended to use at least 6-7 particles per species. If the case occurs that only one particle of a species is present in the cell, this species is skipped in the calculation of  $\mathcal{E}_s$  and  $T$ .

### A. Energy and Momentum Conservation

A detailed discussion of the possible energy and momentum conservation schemes for the particle BGK method can be found in Pfeiffer<sup>8</sup>. For the mixture model, the flow velocity and the thermal energy are determined before the collision ( $\mathbf{u}$  and  $E^{(\text{th})}$ ) and for the provisional post-collision conditions ( $\mathbf{u}^\dagger$  and  $E^{\dagger,(\text{th})}$ ):

$$\mathbf{u} = \frac{\sum_{s=1}^M \sum_{p=1}^{N_s} m_s \mathbf{v}_{p,s}}{\sum_{s=1}^M \sum_{p=1}^{N_s} m_s} \quad (37)$$

$$\mathbf{E}^{(\text{th})} = \sum_{s=1}^M n_s \mathcal{E}_s = \sum_{s=1}^M \sum_{p=1}^{N_s} \frac{m_s (\mathbf{v}_{p,s} - \mathbf{u})^2}{2}. \quad (38)$$

The final post-collision velocity  $\mathbf{v}^*$  of every molecule (whether having undergone a relaxation or not) is then determined from the provisional post-collision velocity  $\mathbf{v}^\dagger$  according to

$$\mathbf{v}^* = \mathbf{u} + (\mathbf{v}^\dagger - \mathbf{u}^\dagger) \sqrt{\frac{E^{(\text{th})}}{E^{\dagger,(\text{th})}}}. \quad (39)$$

## IV. SIMULATION RESULTS

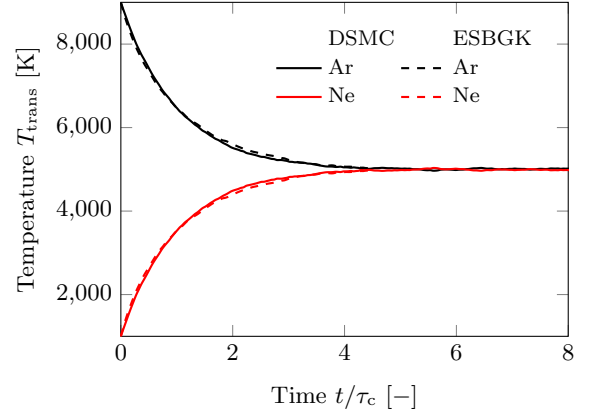
### A. Reservoir Simulations

As a first verification step, simple reservoir (or heat bath) simulations of argon-neon and argon-helium mixtures were performed. These simulations allow to verify the transient relaxation behavior as well as the equilibrium temperature. The gas mixture is initialized at different species temperatures ( $T_{\text{Ar},0} = 9000 \text{ K}$ ,  $T_{\text{He/Ne},0} = 1000 \text{ K}$ ,  $n_{\text{Ar/Ne/He}} = 1 \cdot 10^{23} \text{ m}^{-3}$ ) in a single cell with perfect specular reflection at the boundary. To be able to compare the transient behavior, the time has to be normalized with the respective characteristic relaxation time  $\tau_c$ . It corresponds to the point where the relaxation has progressed to  $1/e$ , for argon the characteristic temperature is  $T_c = 6471.5 \text{ K}$  and the determined relaxation times for the different methods and gases are summarized in Table I.

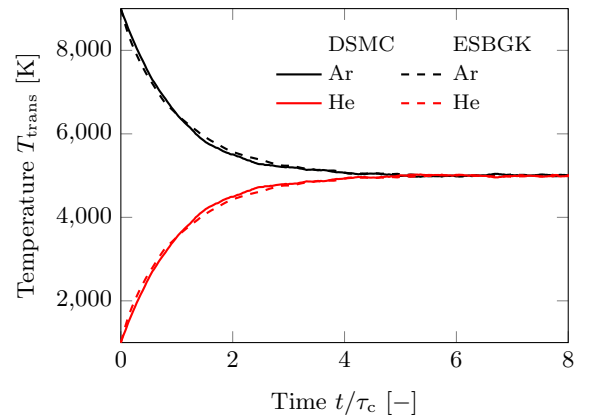
The simulation results using Wilke's mixing rules are shown in Fig. 1 and agree well with DSMC in terms of

TABLE I. Characteristic relaxation times [s] of argon from  $T_{\text{Ar},0} = 9000 \text{ K}$  to  $T_c = 6471.5 \text{ K}$ .

| Ar-Ne                   |                         | Ar-He                   |                         |
|-------------------------|-------------------------|-------------------------|-------------------------|
| DSMC                    | ESBGK                   | DSMC                    | ESBGK                   |
| $2.18689 \cdot 10^{-8}$ | $2.26103 \cdot 10^{-8}$ | $3.88548 \cdot 10^{-8}$ | $1.23369 \cdot 10^{-8}$ |



(a) Argon-Neon



(b) Argon-Helium

FIG. 1. Reservoir (50%:50% mixture): Comparison of species temperature towards thermal equilibrium between DSMC and ESBGK (Brull's model and Wilke's mixing rules). Time is normalized with the respective relaxation time  $\tau_c$ .

the transient behavior as well as the final equilibrium temperature. Slightly better agreement can be seen for the argon-neon mixture due to the lower mass difference of  $m_{\text{Ar}}/m_{\text{Ne}} \approx 2$  as compared to  $m_{\text{Ar}}/m_{\text{He}} \approx 10$ .

### B. Supersonic Couette Flow

The second test case is a supersonic Couette flow. Supersonic conditions were chosen as they push the limits of the methods. Here, the different approaches, Wilke's mixing rules (denoted by Wilke) and the collision integrals (denoted by CollInt) for the determination of the

transport coefficients are compared. The setup is one-dimensional with a height of 1 m and 100 cells in the  $y$ -direction and a single cell in  $x$  and  $z$ . The top and bottom boundaries have a velocity of  $v_{\text{top}} = 350 \text{ m s}^{-1}$  and  $v_{\text{bot}} = -350 \text{ m s}^{-1}$ , respectively. Additionally, diffuse reflection and complete thermal accommodation at a constant wall temperature of  $T_{\text{wall}} = 273 \text{ K}$  is assumed at the boundary. The boundaries in  $x$ - and  $z$ -direction are periodic, meaning that particles leaving on one side reappear on the other. The gas mixture is initialized at  $v_0 = 0$ ,  $T_0 = 273 \text{ K}$ , and  $n = 1.3 \cdot 10^{20} \text{ m}^{-3}$ . After a transient phase, the stationary solution is utilized for comparison with the reference DSMC simulation.

The simulation results of an argon-helium mixture, which represent a challenging case due to the relatively large mass difference, are shown in Fig. 2 and Fig. 3 for a 50%-50% and 75%-25% ratio, respectively. The results using Wilke's mixing rules show good agreement for the number density as well as translational temperature. For the latter, the deviation from the DSMC result is below 2% for the 50%-50% mixture case and below 2.5% for the 75%-25% case. Excellent agreement can be observed using the collision integrals for the number density and temperature, where the temperature deviation is below 0.2% for the 50%-50% and below 0.4% for the 75%-25% case.

The results of a nitrogen-oxygen mixture are shown in Fig. 4. They demonstrate that for lower mass ratios, Wilke's mixing rules achieve very good agreement with the DSMC result.

### C. 70 Degree Blunted Cone

The last verification case is the hypersonic flow around a  $70^\circ$  blunted cone. The geometry of the model, which is based on a wind-tunnel experiment, is shown in Fig. 5. Axisymmetric simulations are performed, where the particle weighting factor increases with an increasing  $y$ . While the DSMC simulations require a particle "cloning"/deletion to ensure that the particle weights of colliding particles are similar, the ESBGK approach can handle different particle weights without additional particle manipulation. The surface of the blunted cone is diffusively reflective and with complete thermal accommodation at a constant wall temperature of  $T_w = 300 \text{ K}$ . Three different test are performed with the inflow conditions shown in Table II to investigate different compositions as well as mass ratios of the included atoms.

TABLE II. Inflow conditions for  $70^\circ$  blunted cone cases.

|        | $n_\infty$ [ $1/\text{m}^3$ ] | $T_\infty$ [K] | $u_\infty$ [m/s] | Composition                            |
|--------|-------------------------------|----------------|------------------|--|
| Case 1 | $7.43 \cdot 10^{20}$          | 13.3           | 1502.57          | $3/4\text{N}-1/4\text{O}$              |
| Case 2 | $7.43 \cdot 10^{20}$          | 13.3           | 1502.57          | $3/4\text{Ar}-1/4\text{He}$            |
| Case 3 | $2.4 \cdot 10^{21}$           | 13.3           | 1502.57          | $1/3\text{N}-1/3\text{O}-1/3\text{Ar}$ |

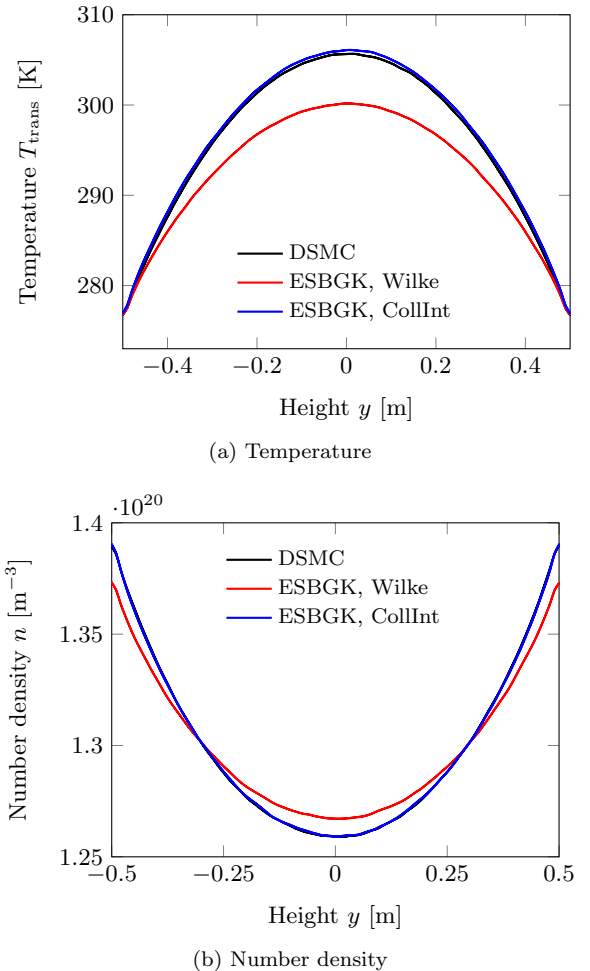
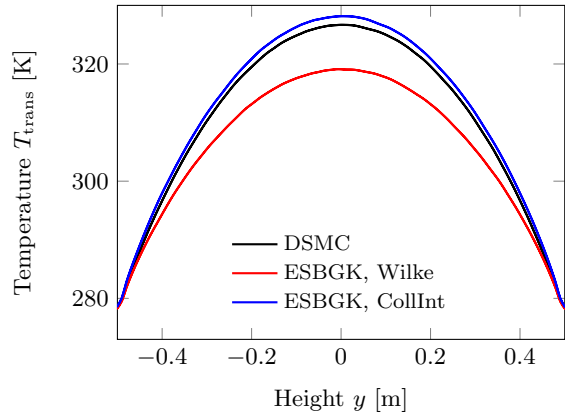


FIG. 2. Comparison of the stationary solution for a supersonic Couette flow for a 50%-50% argon-helium mixture.

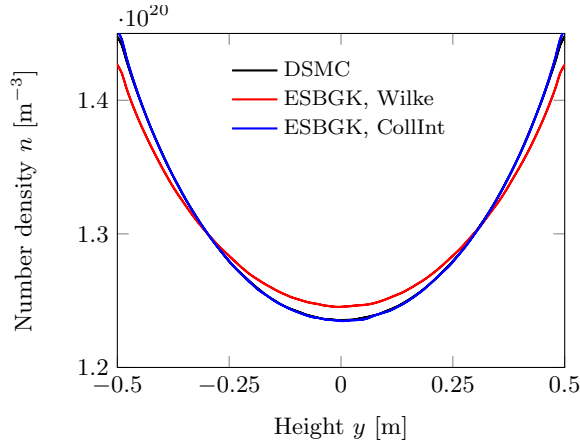
#### 1. Case 1

The first test is performed with an atomic nitrogen-oxygen mixture at a 75%-25% ratio. A comparison of the mean translational temperature of the gas mixture using DSMC and ESBGK is depicted in Fig. 6. The results using Wilke's mixing rules or collision integrals are almost identical in this case and are therefore not shown in this comparison. The ESBGK model predicts an early onset of the temperature increase compared with DSMC, which results in slightly wider shock profiles. However, the overall agreement for with the DSMC result is very good.

The simulation results of the mean flow variables of the mixture as well as the species flow variables over the stagnation stream line are shown in Fig. 7 and Fig. 8, respectively. The overall agreement for both methods with the DSMC result is very good. Again, small differences in the temperature can be observed during the onset of the shock, however, the agreement in the post-shock region is excellent.



(a) Temperature



(b) Number density

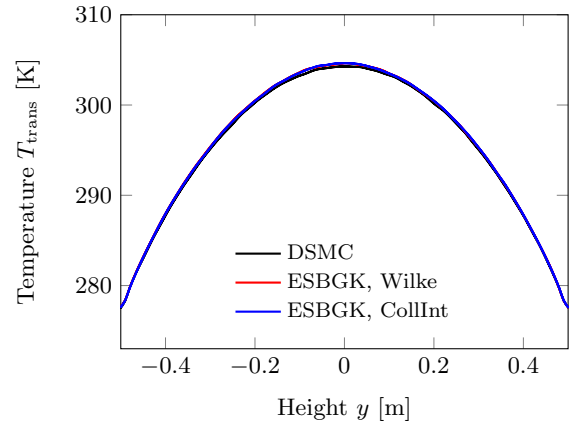
FIG. 3. Comparison of the stationary solution for a supersonic Couette flow for a 75%-25% argon-helium mixture.

The heat flux and pressure on the surface of the cone are depicted in Fig. 9 and Fig. 10 with the points {A,B,C,D} corresponding to the points depicted in Fig. 6. Both show excellent agreement on the flow-facing heat shield as well as the sting further downstream.

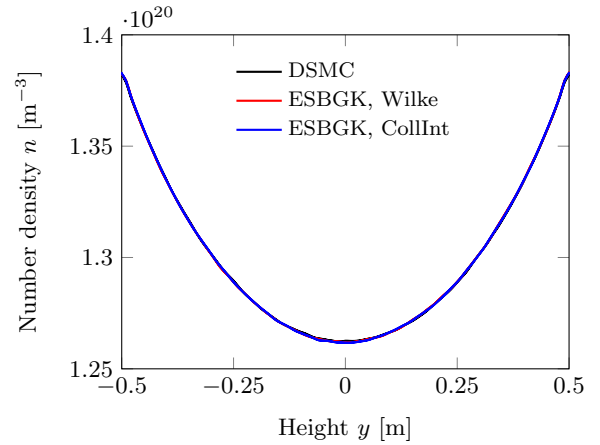
## 2. Case 2

Case 2 is performed with an argon-helium mixture at a 75%-25% ratio. This mixture has a significant higher mass ratio  $m_{Ar}/m_{He} \approx 10$  compared with the first case  $m_{O}/m_{N} \approx 1.14$ . Therefore a greater difference between Wilke's mixing rules and the collision integral approach is expected here. However, the results of the mean flow variables of the mixture (Fig. 11) as well as the species flow variables (Fig. 12) over the stagnation stream line are almost identical for both models. Furthermore, the agreement of both ESBGK models with DSMC regarding the mean flow variables in Fig. 11 is very good, the deviations are only slightly larger than in Case 1.

The differences between the ESBGK models and

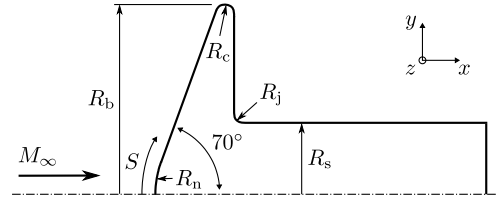


(a) Temperature



(b) Number density

FIG. 4. Comparison of the stationary solution for a supersonic Couette flow for a 50%-50% nitrogen-oxygen mixture.

FIG. 5. Geometry of the  $70^\circ$  blunted cone.  $R_b = 25.0$  mm,  $R_c = 1.25$  mm,  $R_j = 2.08$  mm,  $R_n = 12.5$  mm,  $R_s = 6.25$  mm.  $S$  denotes the arc length along the surface.

DSMC are more pronounced for the individual species in Fig. 12. Nevertheless, the deviation is still relatively small for the large mass ratio. We expect that this difference can be further reduced with more sophisticated models, e.g. by Klingenberg, Pirner, and Puppó<sup>13</sup>, Todorova and Steijl<sup>16</sup>. These will be implemented and compared in the future.

The pressure on the surface depicted in Fig. 13 is almost identical for DSMC and both ESBGK models. The heat flux, however, shows a difference between the

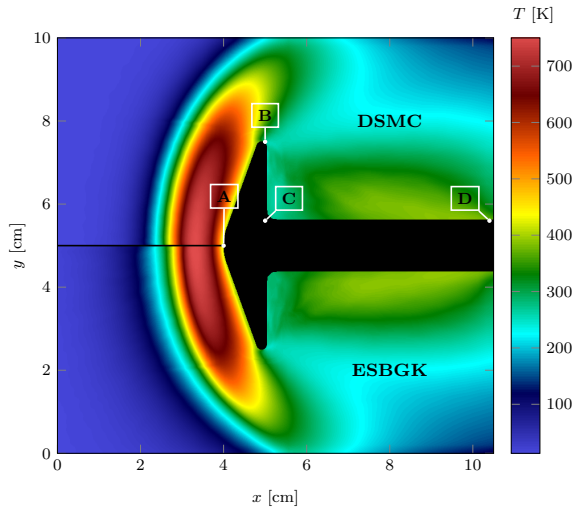


FIG. 6. 70° blunted cone, Case 1: Temperature plots of the flow field using DSMC and ESBGK.

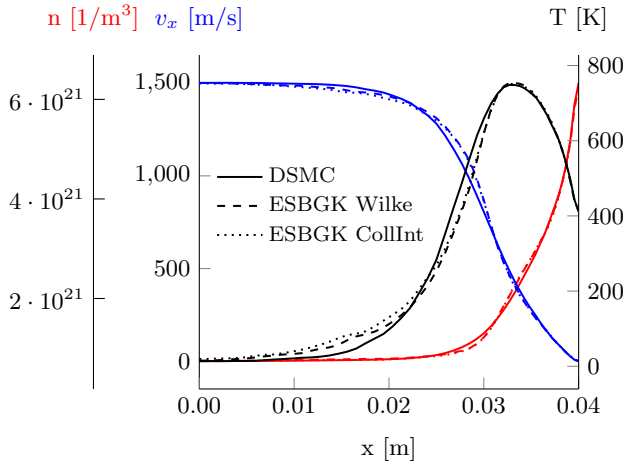


FIG. 7. 70° blunted cone, Case 1: Mixture mean values of gas temperature, velocity in x-direction and number density along stagnation stream line using DSMC and ESBGK.

two ESBGK models, where the collision integral ESBGK model matches the DSMC result very well on the flow-facing heat shield while Wilke's mixing rules show a slight deviation from the DSMC result as shown in Fig. 14. This result was to be expected with regard to the results of the supersonic Couette flow of Section IV B.

### 3. Case 3

The third case is performed with an equal ratio nitrogen-oxygen-argon mixture with mass ratios of  $m_{Ar}/m_N \approx m_{Ar}/m_O \approx 2.6$ . For this case, the product  $\alpha Pr$  is depicted in Fig. 15 to illustrate the changing Prandtl number of the mixture in the flow. The factor  $\alpha Pr$  is ranging between 0.7 and 0.8 in this example.

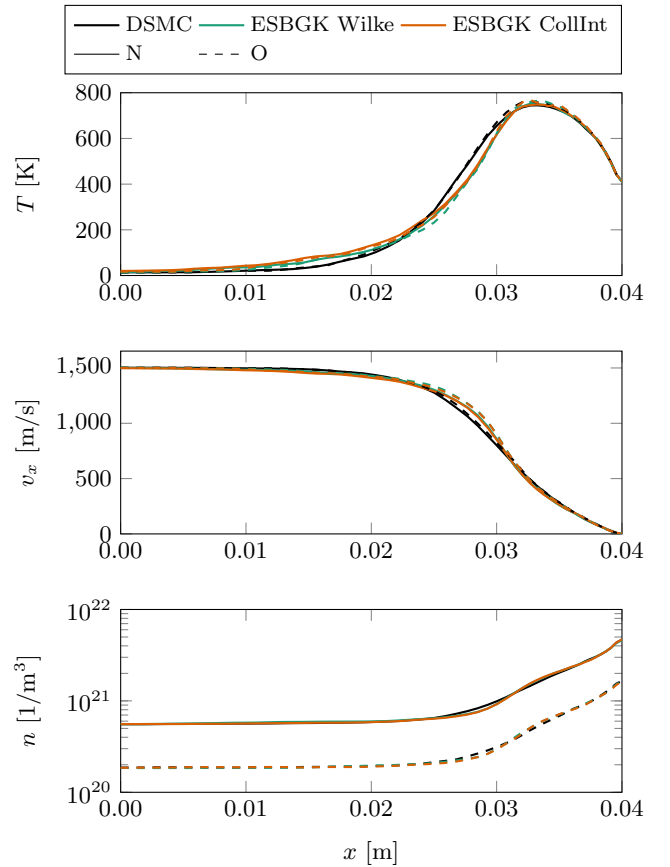


FIG. 8. 70° blunted cone, Case 1: Species temperatures, velocities in x-direction, and number densities along the stagnation stream line using DSMC and ESBGK.

Again, the results of the mean flow variables of the mixture (Fig. 16) as well as the species flow variables (Fig. 17) over the stagnation stream line show a very good agreement between DSMC and both ESBGK models. The DSMC temperature curve of argon as the heaviest species is well reproduced with the ESBGK modeling as depicted in Fig. 17.

The pressure on the surface depicted in Fig. 18 is practically identical again for DSMC and ESBGK. The heat flux of the collision integral ESBGK model matches the DSMC result better than Wilke's mixing rules on the flow-facing heat shield as depicted in Fig. 19. But again, the result with Wilke's mixing rules is also quite good.

A performance comparison for 100 iterations between DSMC as well as ESBGK with Wilke's mixing rules and the collision integral approach is given in Table III for the third case. In cases 1 and 2 the computing time between DSMC and ESBGK was almost the same due to the degree of rarefaction. This has already been described in detail by Pfeiffer, Mirza, and Nizenkov<sup>3</sup>, Pfeiffer<sup>8</sup> and is expected that DSMC will be faster than ESBGK, when the number of collisions is low. In the third test case, however, the density was slightly increased and as shown in Table III, the ESBGK method outperforms DSMC.



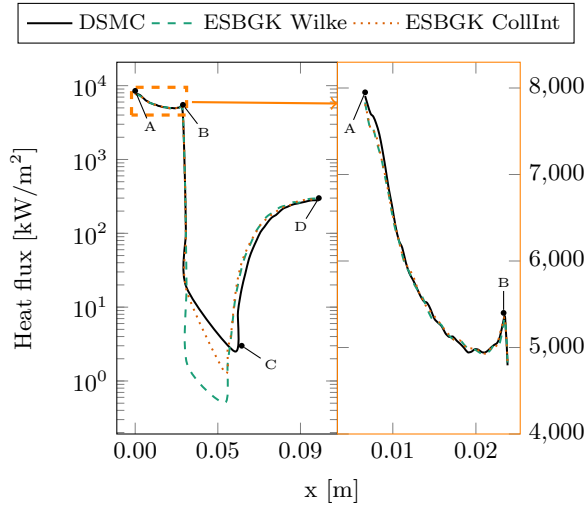


FIG. 9. 70° blunted cone, Case 1: Heat flux on the surface.

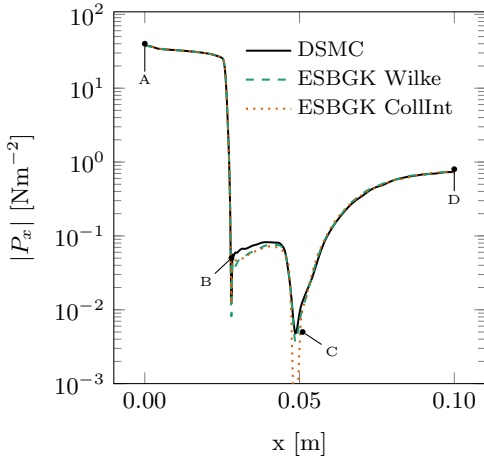


FIG. 10. 70° blunted cone, Case 1: Pressure x direction on the surface.

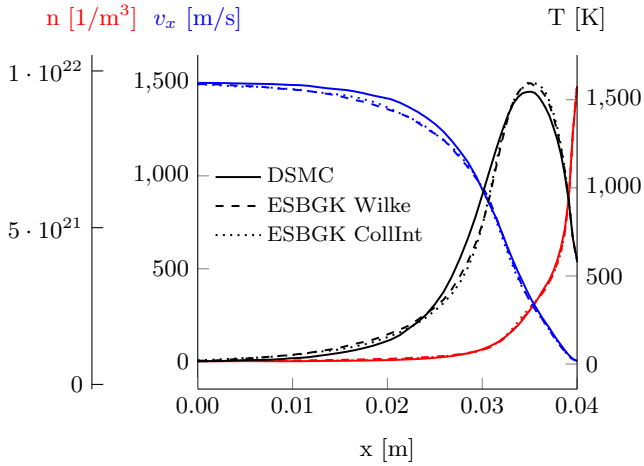


FIG. 11. 70° blunted cone, Case 2: Mixture mean values of gas temperature, velocity in x-direction and number density along stagnation stream line.

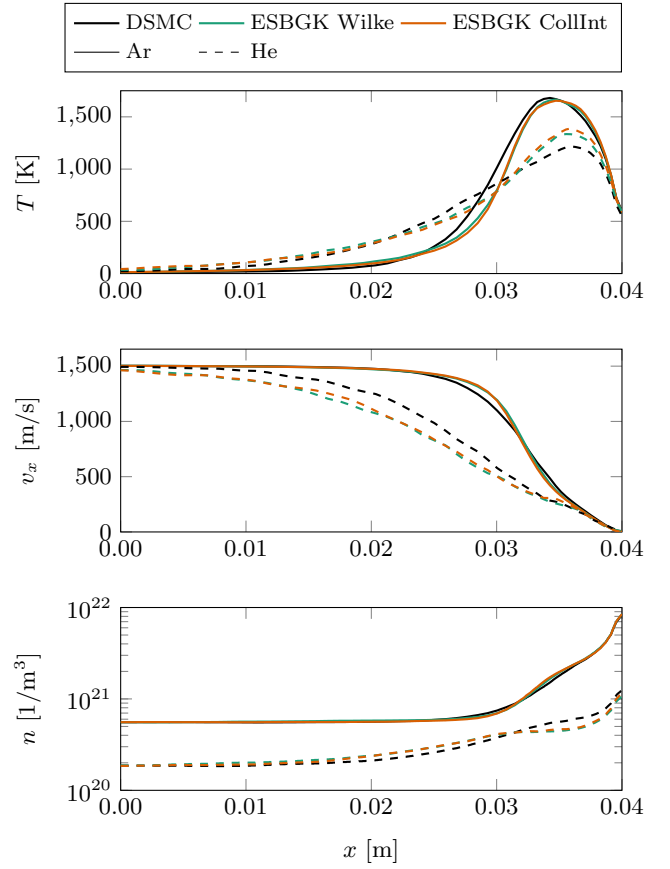


FIG. 12. 70° blunted cone, Case 2: Species temperatures, velocities in x-direction, and number densities along the stagnation stream line using DSMC and ESBGK.

|               | Time step<br>$\Delta t$ [s] | CPU Time /<br>300 iterations<br>[s] | CPU Time /<br>$4.5 \cdot 10^{-5}$ s<br>Simulation<br>time [s] |
|---------------|-----------------------------|-------------------------------------|---|
| DSMC          | $2 \cdot 10^{-8}$           | 112                                 | 840   |
| ESBGK Wilke   | $1.5 \cdot 10^{-7}$         | 55                                  | 55  |
| ESBGK CollInt | $1.5 \cdot 10^{-7}$         | 60                                  | 60  |

TABLE III. Comparison of CPU time between DSMC ( $N_{\text{part}}^{\text{DSMC}} = 6.1 \cdot 10^6$ ) as well as ESBGK ( $N_{\text{part}}^{\text{BGK}} = N_{\text{part}}^{\text{DSMC}}/2$ ) with Wilke's mixing rules and the collision integral model for Case 3. The CPU time is the time per node with 40 cores on an Intel Xeon Platinum 8160 CPU @ 2.10GHz.

This is partly because DSMC needs more particles to resolve the mean free path, and partly because DSMC requires a smaller time step to resolve the collision frequency in this case. As a result, DSMC takes about 14 times longer than ESBGK to achieve the same simulation time for the third test case. The difference in simulation time between ESBGK with Wilke's model and the collision integral model is acceptable considering the increased accuracy in the simulation results.

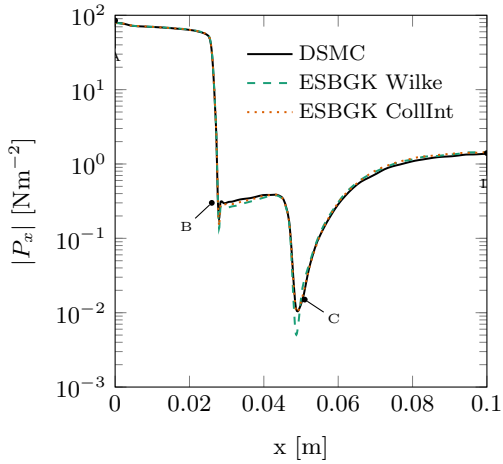


FIG. 13. 70° blunted cone, Case 2: Pressure x direction on the surface.

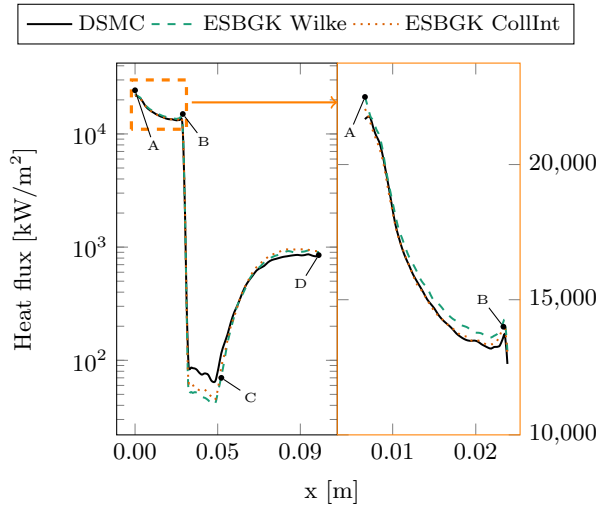


FIG. 14. 70° blunted cone, Case 2: Heat flux on the surface.

## V. CONCLUSION

Multi-species modeling for atomic species in the particle-based ellipsoidal statistical Bhatnagar-Gross-Krook model is implemented using Brull's model<sup>15</sup>. For the determination of the transport coefficients two approaches have been implemented. The first relies on Wilke's mixture rules to determine the mixture properties and the second calculates them from collision integrals (for the Variable Hard Sphere model). The implementation is verified with reservoir test cases, a supersonic Couette flow test case and the hypersonic flow around a 70° blunted cone at different free-stream conditions, and the results are compared with the DSMC method. The collision integral model offers the best agreement overall, and especially when the mass ratio is high (e.g. in an argon-helium mixture) compared to Wilke's mixing rules. However, Wilke's mixing rules

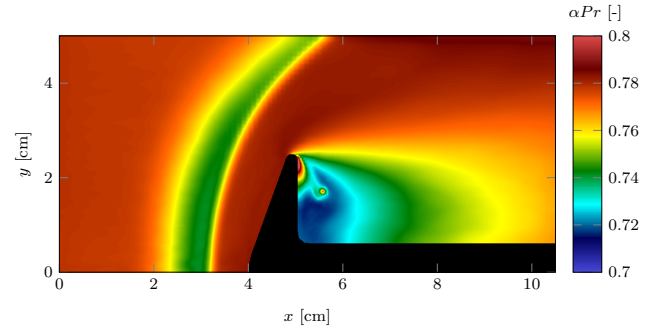


FIG. 15. 70° blunted cone, Case 3: Plot of  $\alpha Pr$  for the collision integral model.

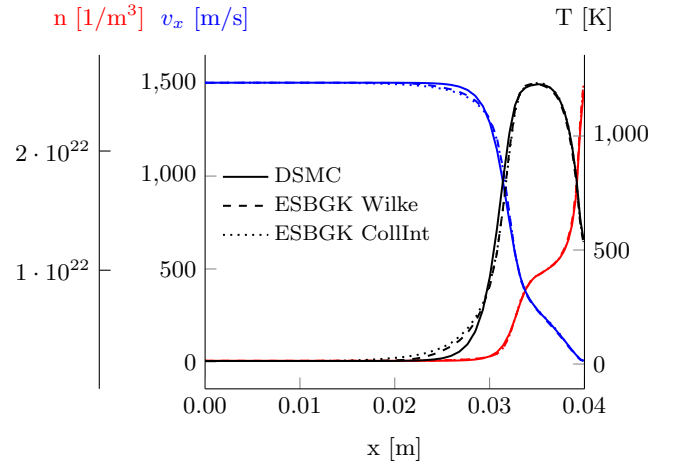


FIG. 16. 70° blunted cone, Case 3: Mixture mean values of gas temperature, velocity in x-direction and number density along stagnation stream line.

show good agreement for smaller mass ratios as demonstrated in supersonic Couette and the 70° blunted cone test cases. Although the calculation of the transport coefficients through the collision integrals is more complex, a first performance comparison of the computational effort suggests that the increase is below 10% compared to Wilke's mixing rules.

The next steps in the development include the investigation of more advanced models for the extension of the kinetic equations (e.g. Todorova and Steijl<sup>16</sup> and Klingenberg, Pirner, and Puppo<sup>13</sup>) and the extension of the current models to diatomic molecules. Looking further ahead, modeling of chemical reactions shall allow the bidirectional coupling with the DSMC method for a multitude of applications such as the simulation of atmospheric entry maneuvers and in-space propulsion.

## ACKNOWLEDGMENTS

The authors gratefully acknowledge the Deutsche Forschungsgemeinschaft (DFG) for funding this research

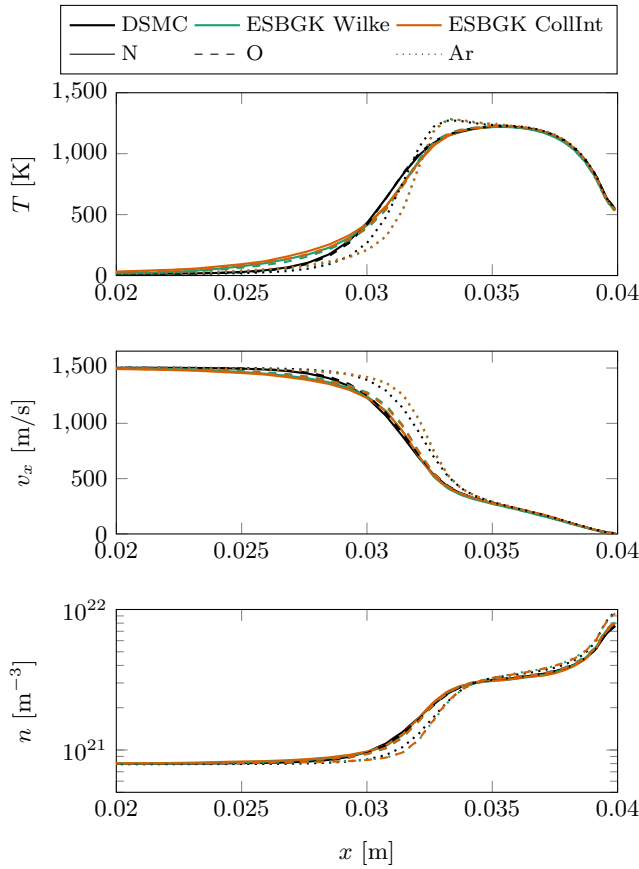


FIG. 17. 70° blunted cone, Case 3: Species temperatures, velocities in x-direction, and number densities along the stagnation stream line using DSMC and ESBGK.

within the project “Partikelverfahren mit Strahlungslöser zur Simulation hochenthalper Nichtgleichgewichts-Plasmen” (project number 93159129). Part of the work was conducted under a program of and funded by the European Space Agency.

- <sup>1</sup>G. A. Bird, *Molecular Gas Dynamics and the Direct Simulation of Gas Flows*, 2nd ed. (Oxford University Press, New York, 1994).
- <sup>2</sup>J. Zhang, B. John, M. Pfeiffer, F. Fei, and D. Wen, “Particle-based hybrid and multiscale methods for nonequilibrium gas flows,” *Advances in Aerodynamics* **1**, 12 (2019).
- <sup>3</sup>M. Pfeiffer, A. Mirza, and P. Nizenkov, “Evaluation of particle-based continuum methods for a coupling with the direct simulation Monte Carlo method based on a nozzle expansion,” *Physics of Fluids* **31**, 073601 (2019).
- <sup>4</sup>P. L. Bhatnagar, E. P. Gross, and M. Krook, “A model for collision processes in gases. I. Small amplitude processes in charged and neutral one-component systems,” *Physical review* **94**, 511 (1954).
- <sup>5</sup>L. H. Holway, “New statistical models for kinetic theory: Methods of construction,” *Physics of Fluids* **9**, 1658–1673 (1966).
- <sup>6</sup>E. M. Shakhov, “Generalization of the Krook kinetic relaxation equation,” *Fluid Dynamics* **3**, 95–96 (1968).
- <sup>7</sup>PICLas is a flexible particle-based plasma simulation suite. Available online at <https://github.com/piclas-framework/piclas>.
- <sup>8</sup>M. Pfeiffer, “Particle-based fluid dynamics: Comparison of different Bhatnagar-Gross-Krook models and the direct simulation

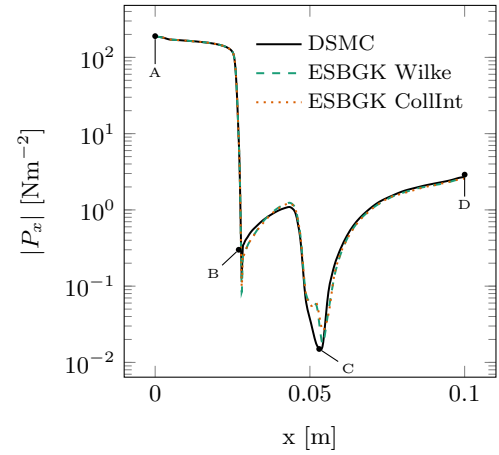


FIG. 18. 70° blunted cone, Case 3: Pressure in x-direction on the surface.

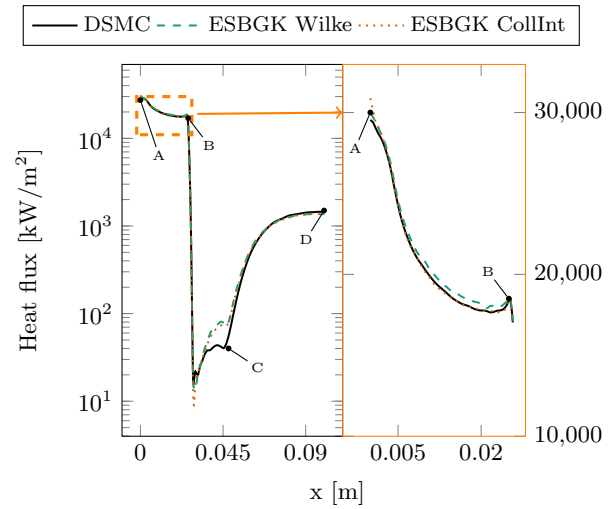


FIG. 19. 70° blunted cone, Case 3: Heat flux on the surface.

- Monte Carlo method for hypersonic flows,” *Physics of Fluids* **30**, 106106 (2018).
- <sup>9</sup>M. Pfeiffer, “Extending the particle ellipsoidal statistical Bhatnagar-Gross-Krook method to diatomic molecules including quantized vibrational energies,” *Physics of Fluids* **30**, 116103 (2018).
- <sup>10</sup>M. Pfeiffer, P. Nizenkov, and S. Fasoulas, “Extension of particle-based BGK models to polyatomic species in hypersonic flow around a flat-faced cylinder,” *AIP Conference Proceedings* **2132**, 100001 (2019).
- <sup>11</sup>P. Andries, K. Aoki, and B. Perthame, “A Consistent BGK-Type Model for Gas Mixtures,” *Journal of Statistical Physics* **106**, 993–1018 (2002).
- <sup>12</sup>C. Klingenberg and M. Pirner, “Existence, uniqueness and positivity of solutions for BGK models for mixtures,” *Journal of Differential Equations* **264**, 702–727 (2018).
- <sup>13</sup>C. Klingenberg, M. Pirner, and G. Puppo, “Kinetic ES-BGK Models for a Multi-component Gas Mixture,” in *Theory, Numerics and Applications of Hyperbolic Problems II*, edited by C. Klingenberg and M. Westdickenberg (Springer International Publishing, 2018) pp. 195–208.
- <sup>14</sup>M. Groppi, S. Monica, and G. Spiga, “A kinetic ellipsoidal BGK model for a binary gas mixture,” *EPL (Europhysics Letters)* **96**,

- 64002 (2011).
- <sup>15</sup>S. Brull, “An ellipsoidal statistical model for gas mixtures,” *Communications in Mathematical Sciences* **13**, 1–13 (2014).
- <sup>16</sup>B. N. Todorova and R. Steijl, “Derivation and numerical comparison of Shakhov and Ellipsoidal Statistical kinetic models for a monoatomic gas mixture,” *European Journal of Mechanics, B/Fluids* **76**, 390–402 (2019).
- <sup>17</sup>C. R. Wilke, “A Viscosity Equation for Gas Mixtures,” *The Journal of Chemical Physics* **18**, 517–519 (1950).
- <sup>18</sup>G. E. Palmer and M. J. Wright, “Comparison of Methods to Compute High-Temperature Gas Viscosity Introduction,” *Journal of Thermophysics and Heat Transfer* **17** (2003), 10.2514/2.6756.
- <sup>19</sup>J. O. Hirschfelder, C. F. Curtiss, and R. B. Bird, *The Molecular Theory of Gases and Liquids*, revised ed ed. (Wiley-Interscience, 1964) p. 1280.
- <sup>20</sup>J. Kestin, K. Knierim, E. A. Mason, B. Najafi, S. T. Ro, and M. Waldman, “Equilibrium and Transport Properties of the Noble Gases and Their Mixtures at Low Density,” (1984).
- <sup>21</sup>M. Capitelli, C. Gorse, S. Longo, and D. Giordano, “Collision integrals of high-temperature air species,” *Journal of Thermophysics and Heat Transfer* **14**, 259–268 (2000).
- <sup>22</sup>M. J. Wright, D. Bose, G. E. Palmer, and E. Levin, “Recommended Collision Integrals for Transport Property Computations Part 1: Air Species,” *AIAA Journal* **43**, 2558–2564 (2005).
- <sup>23</sup>M. J. Wright, H. H. Hwang, and D. W. Schwenke, “Recommended collision integrals for transport property computations part 2: Mars and venus entries,” *AIAA Journal* **45**, 281–288 (2007).
- <sup>24</sup>K. A. Stephani, D. B. Goldstein, and P. L. Varghese, “Consistent treatment of transport properties for five-species air direct simulation Monte Carlo/Navier-Stokes applications,” *Physics of Fluids* **24**, 077101 (2012).
- <sup>25</sup>A. Venkatraman and A. A. Alexeenko, “Binary scattering model for Lennard-Jones potential: Transport coefficients and collision integrals for non-equilibrium gas flow simulations,” *Physics of Fluids* **24** (2012), 10.1063/1.3682375.
- <sup>26</sup>J. Mathiaud and L. Mieussens, “A fokker–planck model of the boltzmann equation with correct prandtl number,” *Journal of Statistical Physics* **162**, 397–414 (2016).
- <sup>27</sup>J. Burt and I. Boyd, “Evaluation of a particle method for the ellipsoidal statistical Bhatnagar-Gross-Krook equation,” in *44th AIAA Aerospace Sciences Meeting and Exhibit* (2006) p. 989.
- <sup>28</sup>C.-D. Munz, M. Auweter-Kurtz, S. Fasoulas, A. Mirza, P. Ortwein, M. Pfeiffer, and T. Stindl, “Coupled Particle-In-Cell and Direct Simulation Monte Carlo method for simulating reactive plasma flows,” *Comptes Rendus Mécanique* **342**, 662–670 (2014).
- <sup>29</sup>S. Fasoulas, C.-D. Munz, M. Pfeiffer, J. Beyer, T. Binder, S. Coplestone, A. Mirza, P. Nizenkov, P. Ortwein, and W. Reschke, “Combining particle-in-cell and direct simulation monte carlo for the simulation of reactive plasma flows,” *Physics of Fluids* **31**, 072006 (2019).
- <sup>30</sup>M. Gallis and J. Torczynski, “Investigation of the ellipsoidal-statistical Bhatnagar-Gross-Krook kinetic model applied to gas-phase transport of heat and tangential momentum between parallel walls,” *Physics of Fluids* **23**, 030601 (2011).
- <sup>31</sup>M. Gallis and J. Torczynski, “The application of the BGK model in particle simulations,” in *34th Thermophysics Conference* (2000) p. 2360.